Nanoscale

Accepted Manuscript

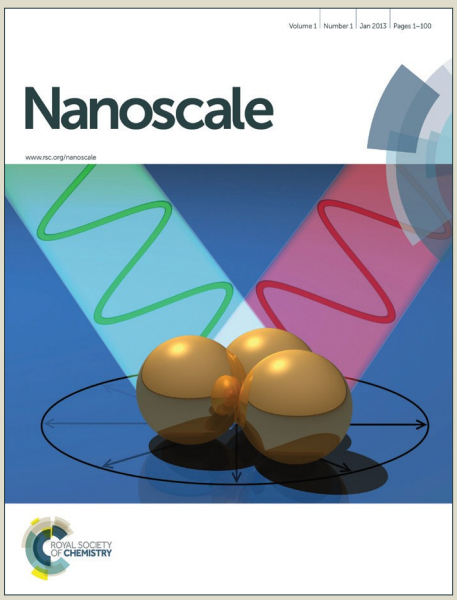

ROYAL SOCIETY OF CHEMISTRY

www.rsc.org/nanoscale

Journal Name

RSCPublishing

ARTICLE

Temporal-spatially transformed synthesis and formation mechanism of gold bellflowers

Cite this: DOI: 10.1039/xoxxoooooox

Received ooth January 2012,
Accepted ooth January 2012

DOI: 10.1039/xoxxoooooox

www.rsc.org/

Jing Lin,[a,c,‡] Molly G. Zhang,[b,‡] Yuxia Tang,[b] Bronte Wen,[b] Hao Hu,[b] Jibing Song,[b] Yijing Liu,[b] Peng Huang,[*,a,b] Xiaoyuan Chen[*,b]

Anisotropic gold nanostructures with unique plasmonic properties, specifically the strong absorption of light in near-infrared region (650~900 nm) due to the excitation of plasmon oscillations, have been widely employed as photothermal conversion agents (PTCAs) for cancer photothermal therapy (PTT). However, the reported PTCAs bear suboptimal photothermal conversion efficiency (η), even gold nanocage (η = 63%), which limits their biomedical applications. Herein, we fabricated gold bellflowers (GBFs) with ultrahigh photothermal conversion efficiency (η = 74%) via a novel liquid/liquid/gas triphasic interface system, using chloroauric acid as a gold source, and *o*-phenetidine as a reducing agent. The well-defined GBFs with multiple-branched petals show adjustable localized surface plasmon resonance (LSPR) from 760 to 1100 nm by tuning the petal length and circular bottom diameter. Originating from the monophasic and biphasic systems used in the creation of gold nanourchins (GNUs) and gold microspheres (GMPs) respectively, the triphasic interface system successfully produced GBFs. The possible formation mechanisms of GNUs, GMPs, and GBFs in the different systems were also investigated and discussed. We found the formation mechanism of GNUs and GBFs followed classical crystallization, while the formation of GMPs followed non-classical crystallization.

Introduction

Plasmonic gold nanoparticles (GNPs), due to their ultrahigh extinction coefficients in the range of 10^9~10^{11} $M^{-1}cm^{-1}$, have been widely used for colorimetric detection, photothermal therapy (PTT) and photoacoustic imaging (PAI).[1-3] The morphology, shape and size of GNPs have shown great potential to tune their localized surface plasmon resonance (LSPR) to the near-infrared (NIR) region.[4] For example, gold nanorods, nanoprisms, and nanoplates have red-shifted LSPR as a result of increased length or edge size.[5-7] Gold nanoshells and nanocages show adjustable LSPR by tuning the shell thickness or core/cavity diameter, respectively.[5-7] Previous studies have illustrated changes in photothermal conversion efficiency (η) following structural alterations.[8, 9] So far, the reported GNPs bear suboptimal η, even gold nanocage (η = 63%), which limits their biomedical applications.[8] Therefore, to further improve the η of GNPs is highly desirable.

The synthesis of GNPs is a cornerstone of nanotechnology, mainly involving chemical, physical and biological methods. Among chemical methods is the synthesis of GNPs through the reduction of chloroauric acid ($HAuCl_4$).[10] The gold ions are reduced to a neutral state upon the introduction of a reducing agent, and the nucleation of gold atoms leads to the formation of GNPs. This is a single liquid phase reaction, the liquid phase being the $HAuCl_4$. Having reported the first metallic nanoparticles in 1847, Faraday fabricated GNPs by reducing gold chloride with phosphorus in carbon disulfide.[11] The currently widely used citrate reduction methods, however, were introduced by Turkevich[12] in 1951 and modified by Frens[13] in the 1970s for the monophasic synthesis of monodisperse spherical GNPs.

A biphasic method for the synthesis of GNPs was introduced in the early 1990s by Brust and Schiffrin *et al.*[14], and has, since then, been frequently employed to fabricate various nanocrystals. Compared with other synthesis methods, the biphasic method has the following advantages[15, 16]: (1) multiple reaction precursors spatially separated in the neighboring organic and aqueous phases; (2) an overlap of the nucleation site of the nanocrystals with the growth stage occurring at the liquid-liquid interface. Due to the success of the biphasic method, the development of triphasic or multiphasic methods may facilitate further alterations in the synthesis of GNPs.

In this study, we deemed that the addition of a phase, and the implementation of a triphasic system, could produce new, potentially more efficient, gold nanostructures. Herein, we employed monophasic, biphasic, and triphasic systems to fabricate GNPs using chloroauric acid as gold source, and *o*-phenetidine as a reducing

agent. Gold nanourchins (GNUs), gold microspheres (GMPs), and gold bellflowers (GBFs) were obtained by monophasic, biphasic, and triphasic systems, respectively. Formation mechanisms of the GNPs obtained from the different phase systems are also investigated and discussed.

Results and Discussion

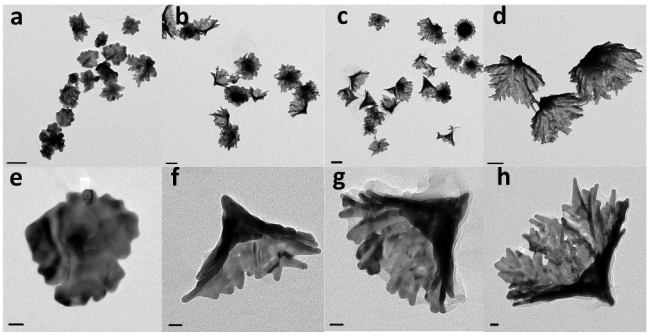

Fig. 1 TEM images of GBFs obtained by triphasic interface synthesis method. GBFs were formed by adding 1 mL (a, e), 2 mL (b, f), 3 mL (c, g), and 4 mL (d, h) of 20 mM *o*-phenetidine in hexane on the top of 5 mL of $HAuCl_4$ aqueous solution (0.8 mM). (a-d) Scale bar =100 nm; (e-h) Scale bar = 20 nm.

In the monophasic system, different volumes of the reducing agent *o*-phenetidine were added to the $HAuCl_4$ aqueous solution. The system was then sonicated. Representative transmission electron microscopy (TEM) images are shown in **Fig. S1**. Interestingly, all of the obtained particles exhibited urchin-like shapes, with highly dense sharp tips 30 nm in length. The diameters of the GNUs was determined to be over 300 nm by measuring 100 randomly selected particles in enlarged TEM images (**Fig. S2a**). At 3 μL of *o*-phenetidine, the size of GNUs was 555.9 ± 93.9 nm. When the volume of *o*-phenetidine increased to 12 μL, the GNU size was 600.6 ± 84.9 nm. **Fig. S2b** shows the UV-vis-NIR absorbance spectra of GNUs with strong absorption in the NIR region. The LSPR of GNUs encompasses the wavelength range of 500-1100 nm.

In the liquid/liquid biphasic system, different volumes (0.5, 1, 2, 3, and 4 mL) of 20 mM *o*-phenetidine in hexane were added to 5 mL of 0.8 mM $HAuCl_4$ aqueous solution. The precursors were spatially separated in the organic (reducing agent *o*-phenetidine in hexane) and aqueous ($AuCl_4^-$) phases. As shown in **Fig. S3**, many irregularly-shaped aggregates were formed when the small volumes (0.5 and 1 mL) of *o*-phenetidine in hexane were added. Increasing the volume of *o*-phenetidine in hexane added to the $HAuCl_4$ aqueous solution resulted in the creation of more GMPs (**Fig. S3c&d**). We suggest that the irregularly-shaped aggregates gradually fused into microspheres with the increased volume of the reducing agent, resulting in particles with a smooth surface.

When 4 mL of 20 mM *o*-phenetidine in hexane was added, the diameter of GMPs was 651.5 ± 92.2 nm (**Fig. S4a**). This was determined by measuring 100 randomly selected particles from enlarged TEM images. As shown in **Fig. S4b**, the particles exhibited an LSPR peak at 615 nm. With the increase in the volume of *o*-phenetidine in hexane, GMPs showed enhanced absorption in the wavelength range of 800-1100 nm.

Based on the monophasic and biphasic systems, the liquid/liquid/gas triphasic interface system was formed with the addition of a gas phase through sonication. The representative TEM images of GBFs are shown in **Fig. 1**. At low levels (1 mL) of *o*-phenetidine in hexane, small flower nanostructures with short petals were formed. With the increase of the volume of *o*-phenetidine in hexane, the products exhibit a well-defined bellflower shape with multiple-branched petals and narrow gaps between the petals. The multiple-branched petals gradually extend and the diameter of circular bottom enlarges as more reducing agent is added. Another aspect of GBFs is their hollow cavity, the wide opening from the conical tip to the scraggly ends of the petals. The base diameter of the circular bottom of the GBFs increased from 111.2 ± 19.9 nm to 338.9 ± 34.8 nm as the volume of reducing agent increased from 1 to 4 mL (**Fig. 2a**). There are more than 10 petals per bellflower and the number increases with increasing the size of GBFs. The GBFs were also accompanied by a significant redshift in the LSPR peak from 760 to 1100 nm (**Fig. 2b**), which makes it highly promising as photothermal conversion agent (PTCA) for PTT using NIR laser irradiation. The η value of the GBFs (3 mL) was determined to be 74%, which is much higher than the other reported PTCAs, such as gold nanocages (63%), GNRs (22%), gold nanoshells (13%), and so on. The high photothermal conversion efficiency of GBFs is ascribed to their unique nanostructure with multiple-branched petals and long narrow gaps between adjacent petals, which greatly enhance the local electromagnetic field and induce a strong plasmonic coupling effect upon incident light, respectively.

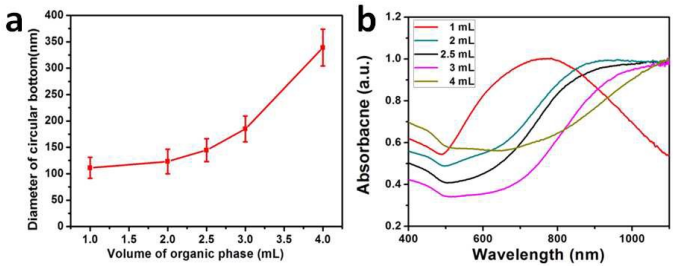

Fig. 2 (a) Diameter change of GBFs with different volumes of *o*-phenetidine in hexane. (b) UV-vis-NIR absorbance spectra of GBFs prepared by different volume of *o*-phenetidine in hexane solutions.

X-ray diffraction (XRD) patterns of GNUs, GMPs, and GBFs were investigated to determine the chemical composition and crystallinity. As shown in **Fig. S5-7**, all three samples exhibit five characteristic diffraction peaks that can be indexed as (111), (200), (220), (311) and (222) crystal planes of face-centered cubic gold, in agreement with the standard card (JCPDS: 04–0784). Despite the different morphologies, all three materials have the same crystallinity. Meanwhile, the plasmonic properties of GNUs, GMPs, and GBFs were compared in **Fig. 3**. GNUs with a diameter of 555.9 ± 93.9 nm exhibited strong absorption in the 500-1100 nm range, with no distinct LSPR peak. GMPs with diameters of 651.5 ± 92.2 nm showed a LSPR peak at 615 nm. GBFs with circular bottoms (the opening of the petals) of 144.6 ± 21.8 nm exhibit a LSPR peak at 900 nm. Thus, it can be seen that the addition of phases to the synthesis of the gold nanomaterial produced more redshifted, and in turn more efficient, nanostructures. The NIR absorption peak of GBFs makes them a promising PTCA for PTT.

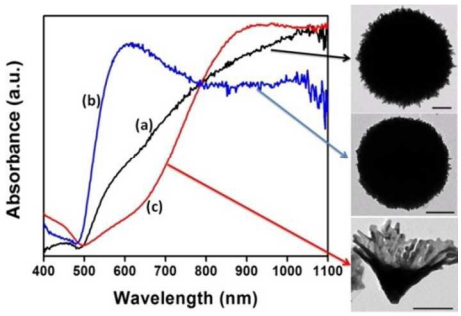

Fig. 3 UV-vis-NIR absorbance spectra and the corresponding TEM images of (a) GNUs, (b) GMPs, and (c) GBFs. Scale bar = 100 nm.

In our study, the synthesis of GBFs through a novel liquid/liquid/gas triphasic interface system originated from the typical two-phase liquid-liquid system. Having experimented with the fabrication of GNUs and GMPs through implementation of the monophasic and biphasic systems respectively, it was determined that neither was capable of producing GBFs. The liquid-liquid biphasic system consisted of solely gold ions and a reducing agent to produce relatively compact GMPs. The addition of the gas phase in the triphasic system introduced a hollow cavity within the nanostructure. Upon ultrasound irradiation, due to the cavitation and nebulization between ultrasound and solvent media, the redox reaction occurred along the liquid/liquid/gas triphase interface with extremely high temperature and pressure.[7] Sonication of the initial gold/hexane solution resulted in the creation of a "bubble" that assisted the growth of the bellflowers. Difference in growth resulted from different GBF orientation from the single nucleation site. The petals of the GBFs were formed through the varied speed of growth of gold colloid along the interface system.

In our case, the reaction precursors spatially separated in the neighboring organic (*o*-phenetidine) and aqueous (gold ions) phases. The reducing agent *o*-phenetidine, due to its amphiphilicity, plays many important roles in liquid/liquid/gas triphasic interface system, such as: i) reducing gold ions into a critical composition of atomic species, ii) capping the surface of newly generated particles, iii) phase-transferring gold ions between hexane and water. In comparison, other reducing agents such as sodium borohydride ($NaBH_4$), *L*-ascorbic acid (*L*-AA), and hydrazine hydrate (N_2H_4•H_2O) were also used in triphasic interface system. Only *o*-phenetidine system shows a consistent phase without distinct layers, other systems display two layers clearly (**Fig. S8**).

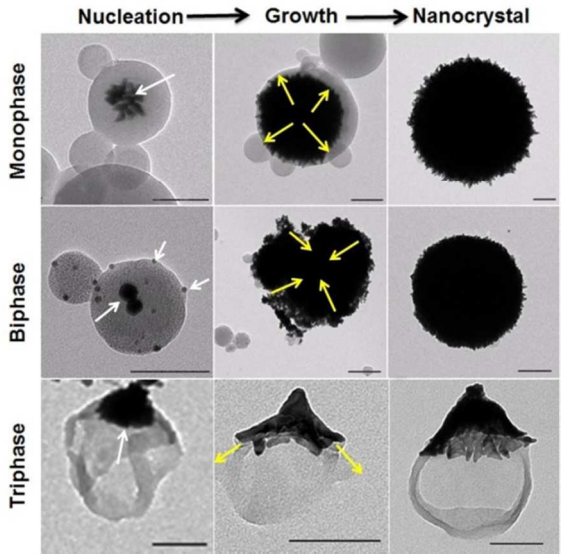

Fig. 4 TEM images of the growth patterns of GNUs, GMPs, and GBFs. In the monophasic and triphasic systems, the formations of GNUs and GBFs followed classical crystallization. In the biphasic system, the formation of GMPs followed non-classical crystallization. Scale bar = 100 nm. White arrows indicate the nucleation locations. Yellow arrows show the growth and self-assembly directions.

The detailed formation mechanisms of the gold nanomaterial in the various phasic systems were observed in the TEM images of nanomaterial growth patterns (**Fig. 4**). In the monophasic system, the formation of GNUs occurs after classical crystallization, a process commonly referred to as the LaMer model.[17-19] At the nucleation stage, gold ions were reduced and entrapped by *o*-phenetidine molecules, some reaching the size of the so-called critical crystal nucleus. The nucleus then gradually grew *via* ion-by-ion attachment. In the biphasic system, the formation of GMPs followed a non-classical crystallization.[19] The nucleation of the gold ions and the formation of the primary GNPs only occurred at the liquid–liquid interface. The subsequent mesocrystals formed through the self-assembly of the primary GNPs. The GMPs were then obtained through the fusion of mesocrystals. In the triphasic system, the formation of GBFs was demonstrated to follow classical crystallization.[19] Upon ultrasound irradiation, due to the cavitation and nebulization between the ultrasound and solvent media, the nucleation took place at the hotspots of vacuum bubbles. The nucleus gradually grew along the liquid/liquid/gas triphasic interface, forming the well-defined bellflower shaped nanostructure.
To further enhance the GBF platform, however, many problems must be considered. One of the main problems is that the GBFs are larger in size than other gold nanostructures.[9] In order to facilitate *in vivo* application, it is essential that the nanostructure be as small as possible, preferably under 100 nm. Additionally, due to its large size as well as the absence of specific biomarkers, it would currently be difficult for GBFs to target tumors through methods other than intratumoral injection.[20] Future work will involve the modification of GBFs for *in vivo* application *via* systemic administration. Moreover, systematic assessment of the toxicity, biocompatibility, pharmacokinetics and biodistribution of the GBFs *in vivo* is also necessary.

The optical property of GBFs also makes it potentially applicable in various other applications in addition to PAI and PTT.[7] One area attracting interest is that of light-triggered drug delivery in regards to cancer. While PTT has proven to assist in tumor ablation, the delivery of drugs is also a crucial aspect of cancer theranostics.[21, 22]

Experimental Section

Monophasic synthesis of gold nanourchins (GNUs)

GNUs were prepared through a monophasic system. 5 mL of $HAuCl_4$ aqueous solution (0.8 mM) was heated at 50 ºC for 5 min. Different volumes (3, 7.5, 9 and12 μL) of *o*-phenetidine (TCI America, >98%) were added to the gold solution. The single-phase liquid system was then sonicated, using the Bransonic® Ultrasonic Cleaner 5510R-DTH system, at 50 ºC for 90 min (operating frequency of 42 ± 6% kHz and power of 135W). The resulting product was collected by centrifugation at 9,000 rpm for 10 min, and was washed three times with deionized water.

Biphasic synthesis of gold microspheres (GMPs)

GMPs were prepared through a two-phase liquid-liquid system involving *o*-phenetidine in hexane on the top of the $HAuCl_4$ aqueous solution. Different volumes (0.5, 1, 2, 3, and 4 mL) of 20 mM *o*-phenetidine were gently added to 5 mL of the $HAuCl_4$ aqueous solution (0.8 mM). The two-phase liquid-liquid system was vigorously stirred for 90 min. The resulting product was then collected and washed as described above.

Triphasic synthesis of gold bellflowers (GBFs)

GBFs were prepared through a liquid/liquid/gas triphasic system arising from an initial two-phase liquid-liquid system involving $HAuCl_4$ and a reducing agent *o*-phenetidine in hexane. $HAuCl_4$ aqueous solution (0.8 mM) was heated at 50 ºC for 5 min. Different volumes (1, 2, 3, and 4 mL) of 20mM *o*-phenetidine in hexane were then added on top of 5 mL of $HAuCl_4$ aqueous solution (0.8 mM). Sonication of the two-phase liquid system (as described above in section 2.1) then produced the third, or gaseous, phase of the triphasic interface system. An additional 60-min sonication under the same condition was performed following the transfer of the solution into an ice-bath. The product was collected by centrifugation at 9000 rpm for 10 min, and was washed three times with deionized water. Subsequently, 100 μL of 10 mM HS-PEG-NH_2 solution was added. The mixture was stirred for 2 h, then centrifuged and washed as described above. The resulting product consisted of PEGylated GBFs in aqueous solution.

Characterization of GNPs

Transmission electron microscopy (TEM) was used to obtain quantitative measurements of particle size, distribution, and morphology. Samples for TEM were prepared by adding 5-10 μL of sample aqueous solution on copper grids supported by 300 mesh carbon film. The grids were air dried at room temperature. Gold nanomaterials were examined under the FEI Tecnai12 transmission electron microscope (FEI, Hillsboro, Oregon) operating at an accelerating voltage of 120 kV. Images were acquired using a Gatan 2k x 2k cooled CCD camera (Gatan, Pleasanton, CA). UV-Vis-NIR spectra were recorded on a Genesys 10S UV-Vis spectrophotometer (Thermo Scientific, Waltham, MA) using quartz cuvettes with an optical path of 1 cm. Distilled water was recorded as the control.

Conclusions

We successfully synthesized gold nanourchins, gold microspheres, and gold bellflowers in monophasic, biphasic, and triphasic systems, respectively, using chloroauric acid as a gold source, and *o*-phenetidine as a reducing agent. The plasmonic properties of the three different products were compared, and the formation mechanisms were discussed. The well-defined GBFs with multiple-branched petals show adjustable LSPR from 760 to 1100 nm by tuning the petal length and circular bottom diameter. The plasmonic property of GBFs serves to reflect their great potential as a PTCA for cancer theranostics. More interestingly, we found the formation mechanism of GNUs and GBFs followed classical crystallization, while the formation of GMPs followed non-classical crystallization.

Acknowledgements

This work was supported by the National Science Foundation of China (81401465, 51573096), and the Intramural Research Program (IRP) of the NIBIB, NIH.

Notes

[a]*Guangdong Key Laboratory for Biomedical Measurements and Ultrasound Imaging, Department of Biomedical Engineering, School of Medicine, Shenzhen University, Shenzhen 518060, China*

[b]*Laboratory of Molecular Imaging and Nanomedicine (LOMIN), National Institute of Biomedical Imaging and Bioengineering (NIBIB), National Institutes of Health (NIH), Bethesda, MD 20892, USA*

[c]*Laboratory of Cellular Imaging and Macromolecular Biophysics (LCIMB), National Institute of Biomedical Imaging and Bioengineering (NIBIB), National Institutes of Health (NIH), Bethesda, MD 20892, USA*

[‡]*These authors contributed equally.*

*Corresponding authors: peng.huang@nih.gov (P. Huang); shawn.chen@nih.gov (X. Chen)

Reference

1 J. F. Lovell, C. S. Jin, E. Huynh, H. Jin, C. Kim, J. L. Rubinstein, W. C. Chan, W. Cao, L. V. Wang and G. Zheng, *Nat. Mater.*, 2011, **10**, 324-332.

2 X. Huang, P. K. Jain, I. H. El-Sayed and M. A. El-Sayed, *Laser Med. Sci.*, 2008, **23**, 217-228.

3 X. Huang, S. Neretina and M. A. El-Sayed, *Adv. Mater.*, 2009, **21**, 4880-4910.

4 Y. Xia and N. J. Halas, *MRS Bulletin*, 2005, **30**, 338-348.

5 E. Ye, K. Y. Win, H. R. Tan, M. Lin, C. P. Teng, A. Mlayah and M.-Y. Han, *J. Am. Chem. Soc.*, 2011, **133**, 8506-8509.

6 P. Huang, L. Bao, C. Zhang, J. Lin, T. Luo, D. Yang, M. He, Z. Li, G. Gao, B. Gao, S. Fu and D. Cui, *Biomaterials*, 2011, **32**, 9796-9809.

7 P. Huang, P. Rong, J. Lin, W. Li, X. Yan, M. G. Zhang, L. Nie, G. Niu, J. Lu, W. Wang and X. Chen, *J. Am. Chem. Soc.*, 2014, **136**, 8307-8313.

8 J. Zeng, D. Goldfeld and Y. Xia, *Angew. Chem. Int. Ed.*, 2013, **52**, 4169-4173.

9 P. Huang, J. Lin, W. Li, P. Rong, Z. Wang, S. Wang, X. Wang, X. Sun, M. Aronova, G. Niu, R. D. Leapman, Z. Nie and X. Chen, *Angew. Chem. Int. Ed.*, 2013, **125**, 14208-14214.

10 L. Dykman and N. Khlebtsov, *Chem. Soc. Rev.*, 2012, **41**, 2256-2282.

11 M. Faraday, *Philos. Trans. R. Soc. London*, 1857, **147**, 145-181.
12 J. Turkevich, P. C. Stevenson and J. Hillier, *Faraday Discuss*, 1951, **11**, 55-75.
13 G. Frens and J. T. G. Overbeek, *J. Colloid. Interface Sci.*, 1972, **38**, 376-387.
14 M. Brust, M. Walker, D. Bethell, D. J. Schiffrin and R. Whyman, *J. Chem. Soc., Chem. Commun.*, 1994, 801-802.
15 P. Huang, J. Lin, Z. Li, H. Hu, K. Wang, G. Gao, R. He and D. Cui, *Chem. Commun.*, 2010, **46**, 4800-4802.
16 J. Yang, E. H. Sargent, S. O. Kelley and J. Y. Ying, *Nat. Mater.*, 2009, **8**, 683-689.
17 V. K. LaMer and R. H. Dinegar, *J. Am. Chem. Soc.*, 1950, **72**, 4847-4854.
18 Y. Xia, Y. Xiong, B. Lim and S. E. Skrabalak, *Angew. Chem. Int. Ed.*, 2009, **48**, 60-103.
19 M. Niederberger and H. Cölfen, *Phys. Chem. Chem. Phys.* , 2006, **8**, 3271-3287.
20 Z. Li, P. Huang, X. Zhang, J. Lin, S. Yang, B. Liu, F. Gao, P. Xi, Q. Ren and D. Cui, *Mol. Pharm.*, 2009, **7**, 94-104.
21 S. M. Janib, A. S. Moses and J. A. MacKay, *Adv. Drug Deliv. Rev.*, 2010, **62**, 1052-1063.
22 S. S. Kelkar and T. M. Reineke, *Bioconjugate Chem.*, 2011, **22**, 1879-1903.